AAS 11-592

TRACKING CONTROL OF NANOSATELLITES WITH UNCERTAIN TIME VARYING PARAMETERS

D. Thakur*and B.G. Marchand†

The focus of this study is an adaptive control scheme that maintains consistent satellite attitude tracking performance in the presence of uncertain time-varying inertia parameters. Potentially large variations in the inertia matrix may occur due to changes in fuel mass, fuel slosh, and deployable appendages such as booms and solar arrays. As such, the assumption of a constant inertia matrix may not suffice for precise tracking maneuvers. The present investigation develops an appropriate description for a class of time-dependent inertia uncertainty. An adaptive control law is implemented to recover closed-loop stability and accurate attitude and angular velocity tracking in the face of such parametric uncertainty.

INTRODUCTION AND MOTIVATION

The attitude control of rigid spacecraft is a widely studied subject, and several stabilizing feedback controllers are available in existing literature[1–3]. Specifically, spacecraft attitude control applications with practical design considerations such as arbitrarily large inertia matrix uncertainty has been the focus of extensive research efforts over the years[2,4–8]. Among these, adaptive control is able to adjust to uncertain parameters using an online identification (estimation) mechanism. While many solutions exist for controlling systems with unknown constant inertia matrix, research in feedback and adaptive control of unknown time-varying inertia matrix is fairly limited.

For instance, mass properties of a spacecraft change with fuel consumption. Although the change in mass may be considered negligible for larger spacecraft, smaller spacecraft such as nanosatellite may exhibit larger variations especially if the propulsive mass accounts for a significant portion of the total mass. Thus, it becomes necessary to model the inertia parameters as time-varying quantities for tracking control applications. Similarly, deployable spacecraft appendages such as antennas, solar arrays, or sensor booms may change the geometry and, subsequently, the inertia matrix description of the satellite. For example, the QuakeSat[9] earth observation nanosatellite and Delfi-C3[10] nanosatellites are both designed with deployable solar panels and communication antennas. The assumption of a constant inertia matrix may not suffice for precise tracking maneuvers for satellite missions with rapid fuel consumption or deployable appendages.

Motivated by the aforementioned issues, the focus of this study is an adaptation mechanism that maintains consistent attitude and angular velocity tracking performance of a satellite in the face of

*PhD Candidate, Department of Aerospace Engineering, The University of Texas at Austin. Email: divs_th@mail.utexas.edu

†Assistant Professor, Department of Aerospace Engineering, The University of Texas at Austin, 210 E. 24th St., Austin, TX 78712. Email: marchand@mail.utexas.edu

uncertain time-varying inertia parameters. The type of time-variation discussed in this study arises during spacecraft appendage deployment and is assumed to be a known quantity. Specifically, the known time-varying component is multiplicative in nature, and the initial inertia parameters are the uncertain quantities. Thus, while the inertia-matrix changes with time, the uncertain component of the matrix remains constant throughout the mission. The spacecraft is assumed to be equipped with a thruster actuation system that enables full three-axis control.

The main objective is to enable the satellite to accurately track a reference trajectory in the presence of arbitrarily large uncertainty for a time-dependent inertia matrix. Adaptive control adjusts to unknown system parameters by updating its controller parameters online using measured signals, and does so while maintaining stability and consistent performance of the system. A vast majority of existing adaptive attitude-control formulations for stabilizing spacecraft attitude tracking dynamics is based upon the classical certainty equivalence (CE) principle. However, CE based adaptive controllers can suffer from performance degradation if the underlying reference signal does not satisfy certain persistence of excitation (PE) conditions[11–13]. A recently introduced noncertainty-equivalence (non-CE) adaptive attitude-tracking control method by Seo and Akella[7] overcomes this limitation and delivers superior performance to the classical CE-based adaptive control scheme. The control formulation provided in the present study is based on the methodology of Seo and Akella. While the original non-CE adaptive control result addresses a constant inertia matrix, the present investigation modifies the original result to handle a time-varying inertia matrix of the multiplicative form stated earlier. The present formulation retains the asymptotic convergence and global stability properties of the original result. Furthermore, it provides the added benefit that the parameter estimation error converges to zero even when the underlying reference signal does not satisfy certain PE conditions. This feature is a direct consequence of the time-varying nature of the inertia matrix and is unavailable in the original non-CE adaptive control result for constant inertia matrix.

Although the selected application of the theoretical development shown here is for nanosatellites, the overall approach is applicable for a spacecraft of any mass and dimension. Furthermore, the application is not limited to spacecraft with time-varying inertia due to deploying appendages. The approach outlined here may be extended to spacecraft exhibiting time-varying inertia properties due to thermal deformation, fuel slosh, or any other physical characteristics, as long as the description of the inertia-matrix conforms to the multiplicative form.

PROBLEM FORMULATION

A dynamical model for the spacecraft tracking problem is formulated using Euler parameters and Euler's rotational equations of motion. Euler parameters, also known as quaternions,[3] provide a nonsingular attitude description and are well suited for spacecraft applications. The Euler parameter kinematic differential equation may be expressed in the form

$$\dot{\mathbf{q}}(t) = \frac{1}{2}\mathbf{E}(\mathbf{q}(t))\boldsymbol{\omega}(t), \tag{1}$$

where the unit quaternion $\mathbf{q}(t) \in \mathbb{R}^4$ consists of scalar and vector components denoted as q_0 and $\mathbf{q_v}$ respectively. Thus, $\mathbf{q} = [q_0,\ \mathbf{q_v}]$ and satisfies the unit-norm constraint ${q_0}^2 + {\mathbf{q_v}}^T\mathbf{q_v} = 1$. The 4×3 matrix $\mathbf{E}(\mathbf{q})$ is defined as

$$\mathbf{E}(\mathbf{q}(t)) = \begin{bmatrix} -\mathbf{q}_v^T \\ q_0\mathbf{I} + [\mathbf{q}_v\times] \end{bmatrix}. \tag{2}$$

where $[\mathbf{q_v}\times]$ is the matrix representation of the linear cross-product operation $\mathbf{q_v}\times$ and is given by the skew-symmetric vector cross-product matrix operator[2]

$$[\mathbf{q_v}\times] = \begin{bmatrix} 0 & -q_{v_3} & q_{v_2} \\ q_{v_3} & 0 & -q_{v_1} \\ -q_{v_2} & q_{v_1} & 0 \end{bmatrix}. \tag{3}$$

In Equation (2), $\boldsymbol{\omega}(t) \in \mathbb{R}^3$ is the angular velocity of the rigid body relative to an inertially fixed reference frame, while $\mathbf{I}$ is the 3×3 identity matrix.

While the attitude kinematical equations describe the time evolution of a rigid spacecraft's orientation in space, Euler's rotational equations of motion address the impact of external control torques. These equations are given by

$$\mathbf{J}(t)\dot{\boldsymbol{\omega}}(t) = -\dot{\mathbf{J}}(t)\boldsymbol{\omega}(t) - \boldsymbol{\omega}(t) \times \mathbf{J}(t)\boldsymbol{\omega}(t) + \mathbf{u}(t), \tag{4}$$

where $\mathbf{J}(t)$ is the time-varying, symmetric positive definite mass-moment of inertia matrix of the spacecraft and $\mathbf{u}(t) \in \mathbb{R}^3$ is the external control torque. Note that for notational convenience, the argument t is hereafter left out.

Tracking Error Dynamics

Consider a spacecraft that is to track the attitude trajectory of a passive target through controlled maneuvers. The spacecraft is required to converge on to the target's quaternion attitude description as well as its angular rotation rates within a specified time period and maintain the convergence for all time thereafter. A control law that satisfies this convergence specification needs constant measured updates for the current attitude of the spacecraft and the desired attitude where the spacecraft should be. The control law aims to drive the attitude and angular velocity tracking errors to zero by adjusting the control effort based on measured updates or estimates of the state.

In order to drive the tracking error to zero, the control law needs a complete dynamical description of the error states. To begin with, a rotation matrix that permits transformation between reference frames is established. The direction cosine matrix, ${}^{\mathcal{B}}\mathbf{C}^{\mathcal{N}}(\mathbf{q})$, denotes a transformation from inertial reference frame $\mathcal{N}$ to body-fixed reference $\mathcal{B}$ (i.e., $\mathcal{N} \longrightarrow \mathcal{B}$), while the argument $\mathbf{q}$ indicates the quaternion that parametrizes the DCM to achieve the desired transformation. Thus, ${}^{\mathcal{B}}\mathbf{C}^{\mathcal{N}}(\mathbf{q})$ can be expressed in terms of the quaternion[3,14] $\mathbf{q}$, that is,

$${}^{\mathcal{B}}\mathbf{C}^{\mathcal{N}}(\mathbf{q}) = ({q_0}^2 - {\mathbf{q_v}}^T\mathbf{q_v})\mathbf{I} + 2\mathbf{q_v}{\mathbf{q_v}}^T - 2\left[\mathbf{q_v}\times\right]. \tag{5}$$

As is often the case, the commanded or reference angular velocity may be prescribed in its own reference frame $\mathcal{R}$. In this case the rotation given by $\mathcal{R} \longrightarrow \mathcal{B}$ is obtained by combining the corresponding rotation matrices, ${}^{\mathcal{B}}\mathbf{C}^{\mathcal{N}}(\mathbf{q})$ and ${}^{\mathcal{R}}\mathbf{C}^{\mathcal{N}}(\mathbf{q}_r)$, through matrix multiplication. The combined rotations can be condensed into a single rotation matrix, ${}^{\mathcal{B}}\mathbf{C}^{\mathcal{R}}(\mathbf{q}_e)$, as follows

$${}^{\mathcal{B}}\mathbf{C}^{\mathcal{R}}(\mathbf{q}_e) = {}^{\mathcal{B}}\mathbf{C}^{\mathcal{N}}(\mathbf{q})\left({}^{\mathcal{R}}\mathbf{C}^{\mathcal{N}}(\mathbf{q}_r)\right)^T. \tag{6}$$

where $\mathbf{q}_e$ denotes the error between the actual quaternion ($\mathcal{N} \xrightarrow{\mathbf{q}} \mathcal{B}$) and desired quaternion ($\mathcal{N} \xrightarrow{\mathbf{q}_r} \mathcal{R}$) states.

The angular velocity tracking error is expressed as

$$\boldsymbol{\omega}_e = \boldsymbol{\omega} - {}^{\mathcal{B}}\mathbf{C}^{\mathcal{R}}(\mathbf{q}_e)\boldsymbol{\omega}_r \tag{7}$$

and provides the error between the angular velocity of the spacecraft and, $\boldsymbol{\omega}_r(t)$, the commanded angular velocity. In order to obtain the tracking error dynamics, the time derivative of Equation (6) and Equation (7) are evaluated along Equation (4). Thus, the attitude error dynamics for a rigid body is given by

$$\dot{\mathbf{q}}(t) = \frac{1}{2}\mathbf{E}(\mathbf{q}_e)\boldsymbol{\omega}_e, \tag{8}$$

and the angular velocity tracking error dynamics are derived as follows

$$\dot{\boldsymbol{\omega}}_e = \mathbf{J}^{-1}\left(-\dot{\mathbf{J}}\boldsymbol{\omega} - [\boldsymbol{\omega}\times]\mathbf{J}\boldsymbol{\omega} + \mathbf{u}\right) + [\boldsymbol{\omega}_e\times] \times {}^{\mathcal{B}}\mathbf{C}^{\mathcal{R}}(\mathbf{q}_e)\boldsymbol{\omega}_r - {}^{\mathcal{B}}\mathbf{C}^{\mathcal{R}}(\mathbf{q}_e)\dot{\boldsymbol{\omega}}_r. \tag{9}$$

The control objective is to track any reference trajectory, $[\mathbf{q}_r, \boldsymbol{\omega}_r]$, for all initial conditions, $[\mathbf{q}(0), \boldsymbol{\omega}(0)]$, assuming full feedback of the signals $[\mathbf{q}, \boldsymbol{\omega}]$ and uncertainty in the time-varying inertia parameters. That is, a control torque $\mathbf{u}$ needs to be designed such that $\lim_{t\to\infty}\left[\mathbf{q}_{e_v},\ \boldsymbol{\omega}_e\right] = 0$, while ensuring that the signals $\boldsymbol{\omega}$ and $\mathbf{q}$ remain bounded at all times. In this way, a tracking control problem has been converted into a stabilization problem for the error states.[2]

Type of Inertia Matrix Considered

A spacecraft with symmetric positive definite time-varying inertia matrix of the form

$$\mathbf{J}(t) = \mathbf{J}_o\boldsymbol{\Psi}(t), \tag{10}$$

is addressed in the subsequent control methods. In Equation (10), $\mathbf{J}_o \in \Re^{3\times 3}$ is a matrix of constant uncertain parameters, and $\boldsymbol{\Psi}(t) \in \Re^{3\times 3}$ is a known matrix function that models the time-variation of $\mathbf{J}(t)$. Additionally, the condition is imposed that $\mathbf{J}_o$ and $\boldsymbol{\Psi}(t)$ are each symmetric and positive definite. The type of uncertainty stated in Equation (10) has a multiplicative nature. A time-varying inertia matrix of this form may be observed in a spacecraft undergoing thermal variations, fuel slosh, or spacecraft appendage deployment such as magnetometer booms, antennas and solar arrays. In this section, a model that demonstrates variations induced during a sensor boom deployment is developed and employed as an application for the control formulation provided in the next section. Note, however, that the control algorithm developed subsequently may be implemented for any inertia-matrix that satisfies Equation (10).

Consider a satellite in the shape of a rectangular prism of dimension $l_1 \times l_1 \times 3l_1$ and mass m_0. The satellite carries two sensor booms which remain in a stowed configuration during launch and subsequent orbit deployment (e.g., the GOES spacecraft mission[15]). The booms may be a lightweight collapsible structure such as the Self-Deploying Astromast[16]. During the course of the mission the booms, which are modeled as two slender bars of length $2l_1$ and mass αm_0 (where $0 < \alpha < 1$), are deployed using a motor-controlled extension. An illustration of the deployment sequence is provided in Figure 1, in which the booms are shown to symmetrically extend through the center of the top and bottom faces of the spacecraft main body.

Assume, for simplicity, that the prism and slender bars each have a uniform mass distribution before, during, and after boom-deployment. Furthermore, assume that the bars are deployed at a constant rate over the duration of τ seconds. Given that the bar's mass to length ratio is $\frac{\alpha m_0}{2l_1}$ and that the bar length, $r(t)$, is obtained by

$$r(t) = \frac{2l_1}{\tau}t, \tag{11}$$

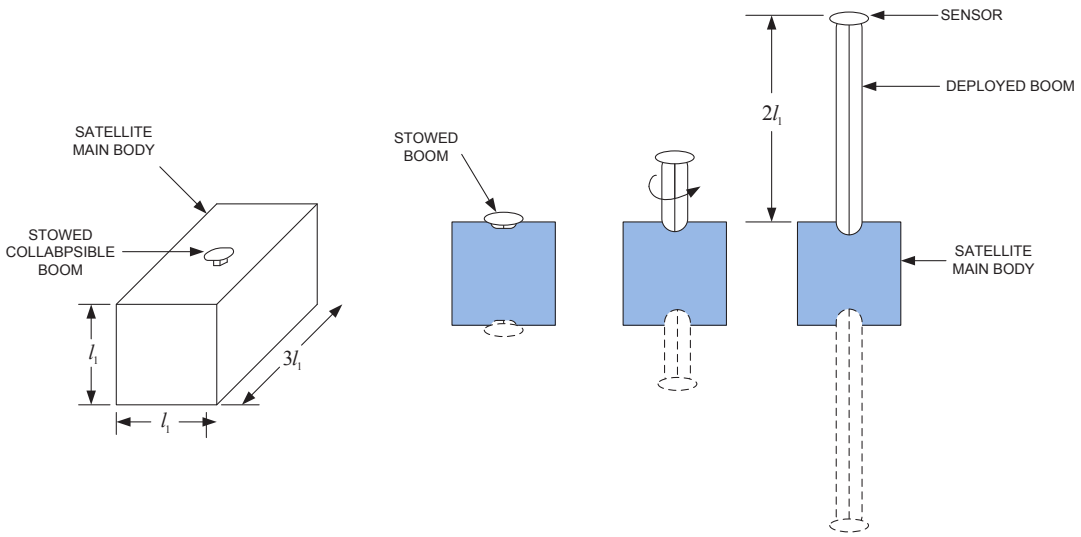

Figure 1: Sensor Boom Deployment Sequence

where $0 \leq t \leq \tau$, it follows that the mass of each bar, $m_p(t)$, increases at a steady rate as shown below

$$m_p(t) = \frac{\alpha m_0}{\tau} t. \tag{12}$$

Consequently, the mass of the prism, $m_c(t)$, simultaneously decreases as described by

$$m_c(t) = m_0 - 2\frac{\alpha m_0}{\tau} t. \tag{13}$$

In Equation (13), m_0 denotes the initial total mass of the prism with stowed booms.

Based on the characteristics of the satellite described in Equations (11)-(13), and through an application of the parallel-axis theorem, the satellite's time-varying inertia parameters are determined about its principle axes in the form of Equation (10) as follows

$$\mathbf{J}_o = \begin{bmatrix} \frac{5}{6} m_0 l_1^2 & 0 & 0 \\ 0 & \frac{5}{6} m_0 l_1^2 & 0 \\ 0 & 0 & \frac{1}{6} m_0 l_1^2 \end{bmatrix}. \tag{14}$$

During sensor boom deployment, for the duration $0 \leq t \leq \tau$, the matrix $\mathbf{\Psi}(t)$ is described as

$$\mathbf{\Psi}(t) = \begin{bmatrix} 1 - 2\frac{\alpha}{\tau} t & 0 & 0 \\ 0 & 1 - \frac{7}{5}\frac{\alpha}{\tau} t + \frac{12}{5}\frac{\alpha}{\tau^2} t^2 + \frac{16}{5}\frac{\alpha}{\tau^3} t^3 & 0 \\ 0 & 0 & 1 + \frac{\alpha}{\tau} t + 12\frac{\alpha}{\tau^2} t^2 + 16\frac{\alpha}{\tau^3} t^3 \end{bmatrix}. \tag{15}$$

At the completion of the boom deployment sequence, that is, at time $t > \tau$, the matrix $\mathbf{\Psi}(t) = \mathbf{\Psi}$ is constant and is described by

$$\mathbf{\Psi}(t) = \begin{bmatrix} 1 - 2\alpha & 0 & 0 \\ 0 & 1 - \frac{7}{5}\alpha + \frac{12}{5}\alpha + \frac{16}{5}\alpha & 0 \\ 0 & 0 & 1 + \alpha + 12\alpha + 16\alpha \end{bmatrix}.$$

In this way, the time-varying matrix is bounded for all time, and preserves the symmetric positive-definite property of the inertia matrix.

NON-CE ADAPTIVE ATTITUDE CONTROL

In this section, an adaptive attitude and angular velocity tracking control algorithm is presented for the problem described by Equation (8) and Equation (9). The control method is based on the non-CE adaptive control results of Seo and Akella,[7] which addresses a constant inertia matrix. The present investigation modifies the control algorithm to handle a time-varying inertia matrix in the form of Equation (10). The main results of the paper are summarized in the theorem below.

Theorem 1. Consider the attitude and angular velocity tracking problem described by Equations (8) and (9) with a time-varying inertia matrix in the form of Equation (10), where $\mathbf{J}_o$ is unknown. Assuming full-state feedback, suppose the adaptive control input is prescribed by

$$\mathbf{u} = \boldsymbol{\Psi}\left(-\mathbf{W}\left(\hat{\boldsymbol{\theta}}+\delta\right)+\mathbf{W}_f\boldsymbol{\Gamma}\mathbf{W}_f^T\left(k_p(\mathbf{q}_{e_v}-\boldsymbol{\omega}_{e_f})+\boldsymbol{\omega}_e\right)\right), \tag{16}$$

$$\dot{\hat{\boldsymbol{\theta}}} = \boldsymbol{\Gamma}\mathbf{W}_f^T\left[(\beta+k_v)\boldsymbol{\omega}_{e_f}+k_p\mathbf{q}_{e_v}\right]-\boldsymbol{\Gamma}\mathbf{W}^T\boldsymbol{\omega}_{e_f}, \tag{17}$$

$$\boldsymbol{\delta} = \boldsymbol{\Gamma}\mathbf{W}_f^T\boldsymbol{\omega}_{e_f}, \tag{18}$$

where the terms k_p, k_v, and $\beta = k_p + k_v$ are positive scalar constants, while $\boldsymbol{\Gamma}$ is a 6×6 positive-definite and diagonal constant matrix. Furthermore, in Equations (16)-(18), the quantity $\mathbf{W}$ is the regressor matrix defined by

$$\begin{aligned}\mathbf{W}\boldsymbol{\theta}^* = &-\boldsymbol{\Psi}^{-1}\mathbf{J}_o\dot{\boldsymbol{\Psi}}\boldsymbol{\omega}-\boldsymbol{\Psi}^{-1}[\boldsymbol{\omega}\times]\mathbf{J}_o\boldsymbol{\Psi}\boldsymbol{\omega}+\mathbf{J}_o\left([\boldsymbol{\omega}\times]{}^{\mathcal{B}}\mathbf{C}^{\mathcal{R}}(\mathbf{q}_e)\boldsymbol{\omega}_r-{}^{\mathcal{B}}\mathbf{C}^{\mathcal{R}}(\mathbf{q}_e)\dot{\boldsymbol{\omega}}_r\right)\\ &+\mathbf{J}_o\left(k_p\beta\mathbf{q}_{e_v}+k_p\dot{\mathbf{q}}_{e_v}+k_v\boldsymbol{\omega}_e\right),\end{aligned} \tag{19}$$

where $\boldsymbol{\theta}^* = [J_{0_{11}}, J_{0_{12}}, J_{0_{13}}, J_{0_{22}}, J_{0_{23}}, J_{0_{33}}]^T$ contains the six unique entries of the matrix $\mathbf{J}_o$. Finally, the variables $\boldsymbol{\omega}_{e_f}\in\mathbb{R}^3$ and $\mathbf{W}_f\in\mathbb{R}^{3\times 6}$ in Equations (16)-(18) are linear, stable variables calculated according to the following first-order filter dynamics

$$\dot{\boldsymbol{\omega}}_{e_f} = -\beta\boldsymbol{\omega}_{e_f}+\boldsymbol{\omega}_e, \tag{20}$$

$$\dot{\mathbf{W}}_f = -\beta\mathbf{W}_f+\mathbf{W}, \tag{21}$$

with arbitrary initial conditions.[7] The adaptive controller stated above ensures boundedness for all closed-loop signals and asymptotic convergence of the tracking error signals $\lim_{t\to\infty}\left[\mathbf{q}_{e_v},\ \boldsymbol{\omega}_e\right]=0$ for all initial conditions $[\mathbf{q}(0),\boldsymbol{\omega}(0)]$ and reference trajectories $[\mathbf{q}_r,\boldsymbol{\omega}_r]$

Proof. Following the approach of Seo and Akella, the dynamics of Equation (9) are transformed to a more desirable parameter-affine form through the careful addition and subtraction of the term $\mathbf{J}\left(k_p\beta\mathbf{q}_{e_v}+k_p\dot{\mathbf{q}}_{e_v}+k_v\boldsymbol{\omega}_e\right)$.[7] That is,

$$\begin{aligned}\dot{\boldsymbol{\omega}}_e = &-k_p\beta\mathbf{q}_{e_v}-k_p\dot{\mathbf{q}}_{e_v}-k_v\boldsymbol{\omega}_e\\ &+\mathbf{J}_o^{-1}\left(\boldsymbol{\Psi}^{-1}\left(\mathbf{u}-\mathbf{J}_o\dot{\boldsymbol{\Psi}}\boldsymbol{\omega}-[\boldsymbol{\omega}\times]\mathbf{J}_o\boldsymbol{\Psi}\boldsymbol{\omega}\right)+\mathbf{J}_o\boldsymbol{\phi}+\mathbf{J}_o\left(k_p\beta\mathbf{q}_{e_v}+k_p\dot{\mathbf{q}}_{e_v}+k_v\boldsymbol{\omega}_e\right)\right),\end{aligned} \tag{22}$$

where $\boldsymbol{\phi} = [\boldsymbol{\omega}\times]{}^{\mathcal{B}}\mathbf{C}^{\mathcal{R}}(\mathbf{q}_e)\boldsymbol{\omega}_r-{}^{\mathcal{B}}\mathbf{C}^{\mathcal{R}}(\mathbf{q}_e)\dot{\boldsymbol{\omega}}_r$ and the time-varying inertia matrix is replaced with its multiplicative form $\mathbf{J}=\mathbf{J}_o\boldsymbol{\Psi}$ as defined earlier in Section . Recognizing the last four terms post-multiplying $\mathbf{J}_o^{-1}$ as the regressor matrix defined in Equation (19), Equation (22) simplifies to

$$\dot{\boldsymbol{\omega}}_e = -k_p\beta\mathbf{q}_{e_v}-k_p\dot{\mathbf{q}}_{e_v}-k_v\boldsymbol{\omega}_e+\mathbf{J}_o^{-1}\left(\boldsymbol{\Psi}^{-1}\mathbf{u}+\mathbf{W}\boldsymbol{\theta}^*\right). \tag{23}$$

Next, define the signal $\boldsymbol{\nu}$ as

$$\boldsymbol{\nu} = \boldsymbol{\Psi}^{-1}\mathbf{u}, \tag{24}$$

and consider the linear filter variable $\boldsymbol{\nu}_f$ obtained from

$$\dot{\boldsymbol{\nu}}_f = -\beta \boldsymbol{\nu}_f + \boldsymbol{\nu}, \tag{25}$$

which is possible since $\boldsymbol{\Psi}$ in Equation (24) is a known, bounded signal. The signal $\boldsymbol{\nu}$ now plays the role of a pseudo-control variable. This is a key step which makes the non-CE adaptive control approach feasible for a time-varying inertia matrix description. With the introduction of $\boldsymbol{\nu}$ and $\boldsymbol{\nu}_f$, the ensuing stability analysis follows closely with the approach of Seo and Akella.[7]

Next, Equation (20) is differentiated on both sides and appropriate substitutions are made using the transformed angular-velocity tracking error dynamics in Equation (23), as well as Equation (21), Equation (24), and Equation (25). The resulting expression is

$$\begin{aligned} \ddot{\boldsymbol{\omega}}_{e_f} = &-\beta \dot{\boldsymbol{\omega}}_{e_f} - k_p \beta \mathbf{q}_{e_v} - k_p \dot{\mathbf{q}}_{e_v} - k_v \left(\dot{\boldsymbol{\omega}}_{e_f} + \beta \boldsymbol{\omega}_{e_f} \right) \\ &+ \mathbf{J}_o^{-1} \left(\dot{\boldsymbol{\nu}}_f + \beta \boldsymbol{\nu}_f + \left(\dot{\mathbf{W}}_f \boldsymbol{\theta}^* + \beta \mathbf{W}_f \boldsymbol{\theta}^* \right) \right). \end{aligned} \tag{26}$$

Upon examining the above expression, note that every term is scaled by the constant β and is accompanied by its corresponding derivative. The expression is rearranged so that the derivatives are on the left hand side of the equation. Then, Equation (26) can be written as a perfect differential, that is,

$$\begin{aligned} &\frac{d}{dt} \left[\dot{\boldsymbol{\omega}}_{e_f} + k_p \mathbf{q}_{e_v} + k_v \boldsymbol{\omega}_{e_f} - \mathbf{J}_o^{-1} \boldsymbol{\nu}_f - \mathbf{J}_o^{-1} \mathbf{W}_f \boldsymbol{\theta}^* \right] \\ &\quad = -\beta \left(\dot{\boldsymbol{\omega}}_{e_f} + k_p \mathbf{q}_{e_v} + k_v \boldsymbol{\omega}_{e_f} - \mathbf{J}_o^{-1} \boldsymbol{\nu}_f - \mathbf{J}_o^{-1} \mathbf{W}_f \boldsymbol{\theta}^* \right). \end{aligned} \tag{27}$$

The solution to Equation (27) is given by

$$\dot{\boldsymbol{\omega}}_{e_f} + k_p \mathbf{q}_{e_v} + k_v \boldsymbol{\omega}_{e_f} - \mathbf{J}_o^{-1} \left(\boldsymbol{\nu}_f + \mathbf{W}_f \boldsymbol{\theta}^* \right) = \boldsymbol{\varepsilon} e^{-\beta t}, \tag{28}$$

where $\boldsymbol{\varepsilon}$ encompasses the initial conditions of all integrable terms

$$\boldsymbol{\varepsilon} = \dot{\boldsymbol{\omega}}_{e_f}(0) + k_p \mathbf{q}_{e_v}(0) + k_v \boldsymbol{\omega}_{e_f}(0) - \mathbf{J}^{-1} \left(\boldsymbol{\nu}_f(0) + \mathbf{W}_f(0) \boldsymbol{\theta}^* \right). \tag{29}$$

If the initial conditions are chosen such that $\boldsymbol{\varepsilon} = 0$, then Equation (28) can be directly solved to obtain an expression for $\dot{\boldsymbol{\omega}}_{e_f}$ that is independent of the angular-velocity tracking error. This is accomplished by selecting $\mathbf{W}_f(0) = 0$, $\boldsymbol{\nu}_f(0) = 0$, and $\boldsymbol{\omega}_{e_f}(0) = \left(\boldsymbol{\omega}_e(0) + k_p \mathbf{q}_{e_v}(0) \right) / k_p$. Thus, by selecting the initial conditions in this manner, it follows that

$$\dot{\boldsymbol{\omega}}_{e_f} = -k_p \mathbf{q}_{e_v} - k_v \boldsymbol{\omega}_{e_f} + \mathbf{J}^{-1} \left(\boldsymbol{\nu}_f + \mathbf{W}_f \boldsymbol{\theta}^* \right). \tag{30}$$

Consistent with the non-CE construction in Seo and Akella,[7] the signal, $\boldsymbol{\delta} \in \mathbb{R}^6$, is introduced that estimates the unknown inertia in conjunction with $\hat{\boldsymbol{\theta}} \in \mathbb{R}^6$. In other words, the estimates for the unknown $\boldsymbol{\theta}^*$ vector are generated by the combined signal $\hat{\boldsymbol{\theta}} + \boldsymbol{\delta}$. Subsequently, the filter signal $\boldsymbol{\nu}_f$ is determined through

$$\boldsymbol{\nu}_f = -\mathbf{W}_f \left(\hat{\boldsymbol{\theta}} + \boldsymbol{\delta} \right), \tag{31}$$

wherein $\boldsymbol{\delta}$ is given by Equation 18.[7] Combining Equations (30) and (31), the dynamical equation for the filter signal, $\boldsymbol{\omega}_{e_f}$ is given by

$$\dot{\boldsymbol{\omega}}_{e_f} = -k_p \mathbf{q}_{e_v} - k_v \boldsymbol{\omega}_{e_f} - \mathbf{J}_o^{-1} \mathbf{W}_f \left(\hat{\boldsymbol{\theta}} + \boldsymbol{\delta} - \boldsymbol{\theta}^* \right). \tag{32}$$

In Equation (32), let $\mathbf{z} = \hat{\boldsymbol{\theta}} + \boldsymbol{\delta} - \boldsymbol{\theta}^*$, which provides the parameter estimation error for the non-CE adaptive control problem. The dynamical equation governing the time evolution of $\mathbf{z}$ is determined through appropriate substitutions of Equations (17), (18), and (30) in the equation $\dot{\mathbf{z}} = \dot{\hat{\boldsymbol{\theta}}} + \dot{\boldsymbol{\delta}}$, thus yielding,

$$\dot{\mathbf{z}} = -\boldsymbol{\Gamma}\mathbf{W}_f{}^T\mathbf{J}_o^{-1}\mathbf{W}_f\mathbf{z}. \tag{33}$$

Consider the following Lyapunov-like function modified from Seo[8]

$$V = \frac{1}{2}\boldsymbol{\omega}_{e_f}^T\boldsymbol{\omega}_{e_f} + \left[\mathbf{q}_{e_v}^T\mathbf{q}_{e_v} + (q_{e_0}-1)^2\right] + \frac{\lambda}{2j_{o_{min}}}\mathbf{z}^T\boldsymbol{\Gamma}^{-1}\mathbf{z},$$

where $\lambda > 0$, and j_{o_min} is the minimum eigenvalue of $\mathbf{J}_o$. The derivative of V is given by

$$\begin{aligned}
\dot{V} &= \boldsymbol{\omega}_{e_f}^T\dot{\boldsymbol{\omega}_{e_f}} - 2\dot{q_{0e}} + \frac{\lambda}{2j_{o_{min}}}\left(\dot{\mathbf{z}}^T\boldsymbol{\Gamma}^{-1}\mathbf{z} + \mathbf{z}^T\boldsymbol{\Gamma}^{-1}\dot{\mathbf{z}}\right), \\
&= \boldsymbol{\omega}_{e_f}^T\left(-k_p\mathbf{q}_{e_v} - k_v\boldsymbol{\omega}_{e_f} - \mathbf{J}_o^{-1}\mathbf{W}_f\mathbf{z}\right) + \mathbf{q}_{e_v}^T\boldsymbol{\omega}_e - \frac{\lambda}{2j_{o_min}}\mathbf{z}^T\mathbf{W}_f^T\mathbf{J}_o^{-1}\mathbf{W}_f\mathbf{z}, \\
&= -k_v\|\boldsymbol{\omega}_{e_f}\|^2 - k_p\boldsymbol{\omega}_{e_f}^T\mathbf{q}_{e_v} - \boldsymbol{\omega}_{e_f}^T\mathbf{J}_o^{-1}\mathbf{W}_f\mathbf{z} + \mathbf{q}_{e_v}^T\left(\dot{\boldsymbol{\omega}}_{e_f} + \beta\boldsymbol{\omega}_{e_f}\right) - \frac{\lambda}{2j_{o_{min}}}\mathbf{z}^T\mathbf{W}_f^T\mathbf{J}_o^{-1}\mathbf{W}_f\mathbf{z} \\
&= -k_v\|\boldsymbol{\omega}_{e_f}\|^2 - k_p\boldsymbol{\omega}_{e_f}^T\mathbf{q}_{e_v} - \boldsymbol{\omega}_{e_f}^T\mathbf{J}_o^{-1}\mathbf{W}_f\mathbf{z} + \mathbf{q}_{e_v}^T\left(-k_p\mathbf{q}_{e_v} - k_v\boldsymbol{\omega}_{e_f} - \mathbf{J}_o^{-1}\mathbf{W}_f\mathbf{z} + \beta\boldsymbol{\omega}_{e_f}\right) \\
&\quad - \frac{\lambda}{2j_{o_{min}}}\mathbf{z}^T\mathbf{W}_f^T\mathbf{J}_o^{-1}\mathbf{W}_f\mathbf{z} \\
&= -k_v\|\boldsymbol{\omega}_{e_f}\|^2 - k_p\|\mathbf{q}_{e_v}\|^2 - \boldsymbol{\omega}_{e_f}^T\mathbf{J}_o^{-1}\mathbf{W}_f\mathbf{z} - \mathbf{q}_{e_v}^T\mathbf{J}_o^{-1}\mathbf{W}_f\mathbf{z} - \frac{\lambda}{2j_{o_{min}}}\mathbf{z}^T\mathbf{W}_f^T\mathbf{J}_o^{-1}\mathbf{W}_f\mathbf{z} \\
&\leq -\frac{2}{3}k_v\|\boldsymbol{\omega}_{e_f}\|^2 - \frac{2}{3}k_p\|\mathbf{q}_{e_v}\|^2 - \frac{\lambda}{3}\|\mathbf{J}_o^{-1}\mathbf{W}_f\mathbf{z}\|^2 \\
&\quad \frac{-k_v}{3}\left(\|\boldsymbol{\omega}_{e_f}\|^2 + \frac{3}{k_v}\boldsymbol{\omega}_{e_f}^T\mathbf{J}_o^{-1}\mathbf{W}_f\mathbf{z} + \frac{\lambda}{k_v}\|\mathbf{J}_o^{-1}\mathbf{W}_f\mathbf{z}\|^2\right) \\
&\quad \frac{-k_p}{3}\left(\|\mathbf{q}_{e_v}\|^2 + \frac{3}{k_p}\mathbf{q}_{e_v}^T\mathbf{J}_o^{-1}\mathbf{W}_f\mathbf{z} + \frac{\lambda}{k_p}\|\mathbf{J}_o^{-1}\mathbf{W}_f\mathbf{z}\|^2\right) \\
&\leq -\frac{2}{3}k_v\|\boldsymbol{\omega}_{e_f}\|^2 - \frac{2}{3}k_p\|\mathbf{q}_{e_v}\|^2 - \frac{\lambda}{3}\|\mathbf{J}_o^{-1}\mathbf{W}_f\mathbf{z}\|^2 \\
&\leq 0,
\end{aligned}$$

which indicates that $\dot{V} \leq 0$ and consequently $\boldsymbol{\omega}_{e_f}, \mathbf{q}_{e_v}, \mathbf{z} \in \mathcal{L}_\infty$, that is, the closed loop signals are bounded. Since the integral of $\dot{V}$ exists and is finite, $\mathbf{q}_{e_v}, \boldsymbol{\omega}_{e_f}, \mathbf{J}_o^{-1}\mathbf{W}_f\mathbf{z} \in \mathcal{L}_2 \cap \mathcal{L}_\infty$ and subsequently, $\left(\dot{\mathbf{q}}_{e_v}, \dot{\boldsymbol{\omega}}_{e_f}, \frac{d}{dt}\left(\mathbf{W}_f\mathbf{z}\right)\right) \in \mathcal{L}_\infty$, which permit the following conclusion based on Barbalat's lemma

$$\lim_{t\to\infty}\begin{bmatrix} \mathbf{q}_{e_v}(t) \\ \boldsymbol{\omega}_{e_f}(t) \\ \mathbf{J}_o^{-1}\mathbf{W}_f\mathbf{z}(t) \end{bmatrix} = 0. \tag{34}$$

Furthermore, by invoking Equation (32), it becomes clear that $\lim_{t\to\infty} = \boldsymbol{\omega}_e$.

Finally, it remains to extract the actual controller $\mathbf{u}$ from the filtered signal $\boldsymbol{\nu}_f$. This can be done simply through the substitution

$$\mathbf{u} = \boldsymbol{\Psi}\left(\dot{\boldsymbol{\nu}}_f + \beta\boldsymbol{\nu}_f\right), \tag{35}$$

which can be expanded through substitutions of Equations (17), (18), (21), and (31) to recover the expression in Equation (16).

NUMERICAL SIMULATIONS

In this section, two sets of numerical simulation studies are performed to validate the performance of the adaptive control algorithm in the presence of uncertainty in time varying-inertia parameters. The first set of simulations is provided for a non-PE reference angular velocity profile, while the second set is for a PE reference signal. For this specific example, the quantities $\mathbf{J}_o$ and $\mathbf{\Psi}$ are given by Equations (14) and (15) where

$$m_0 = 30 \text{ kg}, \quad l = 0.2 \text{ m}, \quad \alpha = 0.1, \quad \tau = 200 \text{ seconds} \ . \tag{36}$$

An initial error of 30% is assumed in the knowledge of $\mathbf{J}_o$, that is

$$\hat{\boldsymbol{\theta}}(0) + \boldsymbol{\delta}(0) = 1.3\boldsymbol{\theta}^*. \tag{37}$$

The actual and commanded initial conditions are

$$\begin{aligned}
\mathbf{q}(0) &= \left[\ 0.9487, \quad 0.1826, \quad 0.1826, \quad 0.18268 \ \right]^T, \\
\boldsymbol{\omega}(0) &= \left[\ 0, \quad 0, \quad 0 \ \right]^T \text{ rad/s}, \\
\mathbf{q}_r(0) &= \left[\ 1, \quad 0, \quad 0, \quad 0 \ \right]^T.
\end{aligned}$$

The reference angular velocity profile is updated at each simulation time. In addition, as mentioned previously, the initial filter-states are as follows

$$\mathbf{W}_f(0) = 0, \qquad \boldsymbol{\omega}_f(0) = \frac{\boldsymbol{\omega}_e(0) + k_p \mathbf{q}_{v_e}(0)}{k_p}.$$

Non-PE Reference Trajectory

In this set of simulations, the following non-PE reference trajectory is simulated:

$$\boldsymbol{\omega}_r = 0.1\cos(t)(1 - e^{0.01t^2}) + (0.08\pi + 0.006\sin(t))te^{-0.01t^2} \cdot \left[\ 1 \quad 1 \quad 1 \ \right]^T \text{ rad/s}, \tag{38}$$

which is obtained from the example provided in Seo and Akella. The gain values are selected as $k_p = 0.08$, $k_v = 0.07$, and $\mathbf{\Gamma} = \text{diag}\left\{100, 0.01, 0.01, 200, 0.01, 100\right\}$. A simulation is performed for a period of 200 seconds using the aforementioned parameter values.

The results of the simulation are illustrated in Figure 2. While the attitude and angular velocity errors both asymptotically converge to zero as expected, the convergence of of the parameter estimation norm to zero is rather unexpected. In general, the non-PE nature of the reference trajectory prohibits the convergence of the parameter estimates to their true values. However, there is added persistence of excitation due to the time-varying term $\mathbf{\Psi}$ in the inertia matrix. This allows the parameter estimates to converge to their true values even in the case of a non-PE reference trajectory. The control torques remain time-varying and increase in amplitude to accommodate the variations in the inertia parameters and ensure faithful tracking of the reference trajectory for the entire simulation period. The constant matrix $\mathbf{\Gamma}$ is used to tune the rate of the estimation error convergence as well as improve the attitude and angular velocity error convergence.

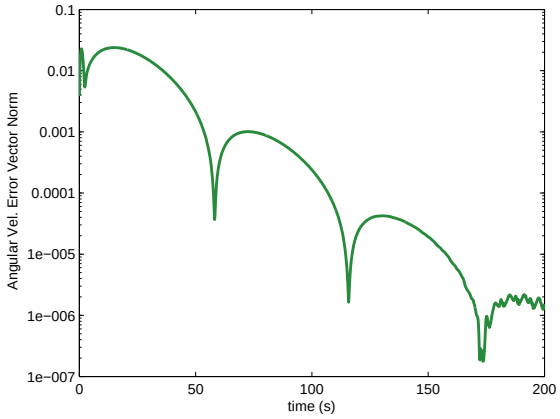

(a) Norm of angular velocity error vector $\|\boldsymbol{\omega}_e\|$

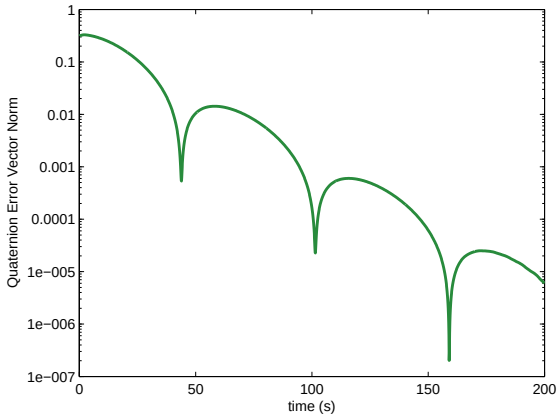

(b) Norm of quaternion error vector $\|\mathbf{q}_{e_v}\|$

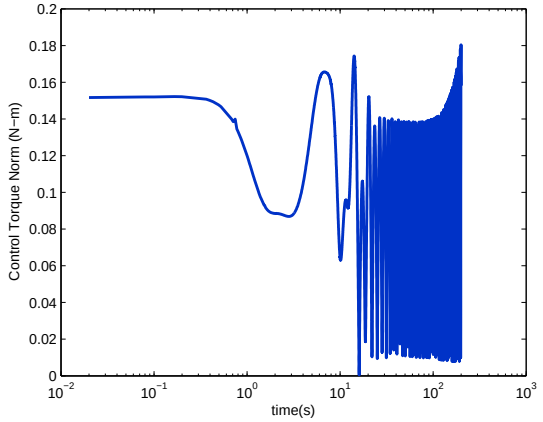

(c) Norm of control vector $\|\mathbf{u}\|$

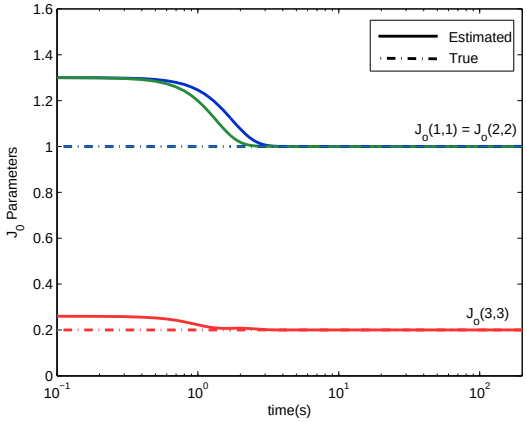

(d) Parameter estimates converge to true values due to additional persistence of excitation introduced by $\boldsymbol{\Psi}(t)$

Figure 2: Non-CE adaptive tracking-control simulation for a spacecraft with time-varying inertia parameters tracking a non-PE reference signal.

PE Reference Trajectory

In this set of simulations, a PE reference trajectory given by

$$\boldsymbol{\omega}_r = \left[\begin{array}{ccc} \cos(t) + 2, & 5\cos(t), & \sin(t) + 2 \end{array} \right]^T \text{ rad/s}, \tag{39}$$

is simulated. As in the first set of simulations, this reference trajectory is obtained from the example provided in Seo and Akella. The gain values are selected as $k_p = 0.8$, $k_v = 0.8$, and $\boldsymbol{\Gamma} = \text{diag}\{1, 0.001, 0.001, 1, 0.001, 1\}$. As before, the duration of the simulation is 200 seconds. The results of the simulation are illustrated in Figure 3. The attitude and angular velocity errors both asymptotically converge to zero as expected. For a PE reference trajectory, the convergence of the parameter estimation norm is expected and clearly evident from the illustration.

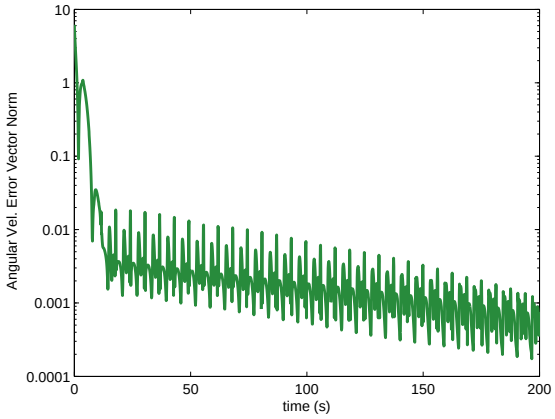

(a) Norm of angular velocity error vector $\|\boldsymbol{\omega}_e\|$

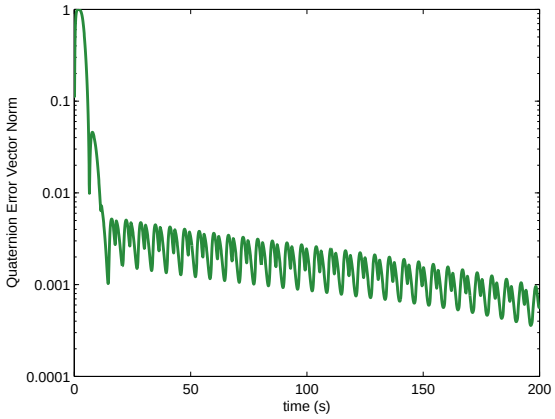

(b) Norm of quaternion error vector $\|\mathbf{q}_{e_v}\|$

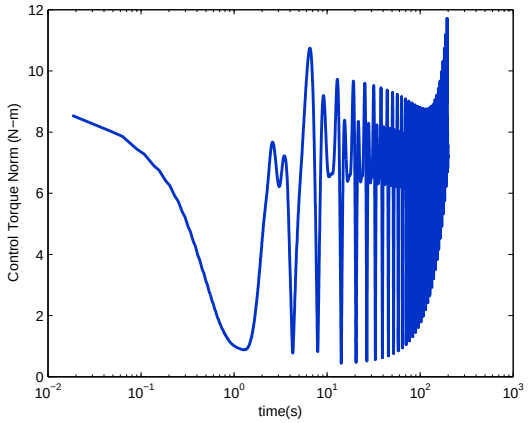

(c) Norm of control vector $\|\mathbf{u}\|$

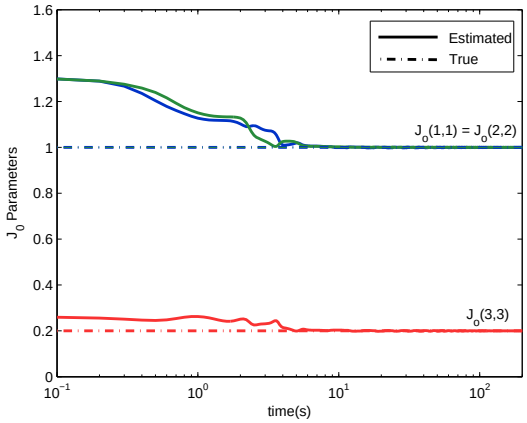

(d) Parameter estimates converge to true values

Figure 3: Non-CE adaptive tracking-control simulation for a spacecraft with time-varying inertia parameters tracking a PE reference signal.

CONCLUSIONS

The problem of spacecraft attitude-tracking in the presence of arbitrarily large multiplicative uncertainties for a time-varying inertia matrix is addressed. A noncertainty-equivalence adaptive controller is employed for consistent angular velocity and attitude tracking. Numerical simulations for non-persistently exciting and persistently exciting reference trajectories are performed, which demonstrate asymptotic convergence of the attitude and angular-velocity tracking errors to zero. Moreover, the persistence of excitation induced by the time-varying inertia parameters enables the parameter estimation error norm to also converge to zero even when the underlying reference trajectory itself does not satisfy persistence of excitation conditions.

ACKNOWLEDGEMENTS

This research was carried out at The University of Texas at Austin. The authors would like to extend their gratitude to Dr. Srikant Sukumar for his guidance and technical feedback.

REFERENCES

[1] B. Wie and P. M. Barba, "Quaternion Feedback for Spacecraft Large Angle Maneuvers," *Journal of Guidance and Control*, Vol. 8, No. 3, 1985, pp. 360–365.

[2] J. T. Wen and K. Kreutz-Delgado, "The Attitude Control Problem," *IEEE Trans. on Automatic Control*, Vol. 36, No. 10, 1991, pp. 1148–1162.

[3] H. Schaub and J. Junkins, *Analytical Mechanics of Space Systems*, ch. 3. AIAA Education Series, 2003.

[4] B. T. Costic, D. M. Dawson, M. S. de Queiroz, and V. Kapila, "Quaternion-Based Adaptive Attitude Tracking Controller Without Velocity Measurements," *Journal of Guidance, Control, and Dynamics*, Vol. 24, No. 6, 2001, pp. 1214–1222.

[5] J. Ahmed and D. S. Bernstein, "Globally Convergent Adaptive Control of Spacecraft Angular Velocity Without Inertia Modeling," *American Control Conference*, Vol. 3, No. 1, 1999, pp. 1540–1544.

[6] A. Astolfi and R. Ortega, "Immersion and Invariance: A New Tool for Stabilization and Adaptive Control of Nonlinear Systems," *IEEE Trans. on Automatic Control*, Vol. 48, No. 2, 2003, pp. 590–606.

[7] D. Seo and M. R. Akella, "High-Performance Spacecraft Adaptive Attitude-Tracking Control Through Attracting-Manifold Design," *Journal of Guidance, Control, and Dynamics*, Vol. 31, No. 4, 2008, pp. 884–891.

[8] D. E. Seo, *Noncertainty Equivalent Nonlinear Adaptive Control and its Application to Mechanical and Aerospace Systems*. PhD thesis, The University of Texas at Austin, August 2007.

[9] *QuakeSat Nano-Satellite*. `http://www.quakefinder.com/services/quakesat-ssite/`.

[10] *The Delfi-C3 Project*. `http://www.delfic3.nl/index.php?option=com_content&task=view&id=67&Itemid=109`.

[11] J. J. E. Slotine and W. Li, *Applied Nonlinear Control*. Prentice-Hall, 1991.

[12] K. J. Aström and B. Wittenmark, *Adaptive Control*, ch. 3. Addison-Wesley Publishing Co., Inc., 1995.

[13] P. A. Ioannou and J. Sun, *Robust Adaptive Control*, ch. 4. Prentice-Hall, 1995.

[14] M. D. Shuster, "A Survey of Attitude Representation," *The Journal of Astronautical Sciences*, Vol. 41, No. 4, 1993, pp. 439–517.

[15] *Space Systems Loral*, "GOES I-M Databook," `http://goes.gsfc.nasa.gov/text/goes.databook.html`, 1996.

[16] *Northrop Grumman*, "Astromast," `http://www.as.northropgrumman.com/products/aa_astromast/index.html`.